



PERGAMON

Mechanics and Physics of Solids 47 (1999) 81–97

JOURNAL OF THE
MECHANICS AND
PHYSICS OF SOLIDS

Fatigue crack growth in ferroelectrics driven by cyclic electric loading

Ting Zhu, Wei Yang*

Department of Engineering Mechanics, Tsinghua University, Beijing 100084, China

Received 12 November 1997; revised 19 June 1998

Abstract

Fatigue crack growth has been observed recently in ferroelectrics under cyclic electric loading. Does the crack grow by electric breakdown, or by the stress field near the crack tip? The present paper provides a mechanistic explanation for the electric-field-induced fatigue crack growth. The non-uniform electric field near an insulated crack tip might cause domain switching which in turn produces a concentrated stress field characterized by a stress intensity factor. For ferroelectrics poled along a direction perpendicular to the crack, we are able to show quantitatively that: (1) the stress intensity factor under a negative electric field is nine times as large as the stress intensity factor under a positive electric field; (2) the crack starts to grow if the stress intensity factor is higher than the fracture toughness of the material, but the stress intensity factor decreases as the crack extends and eventually results in crack arrest; (3) by reversing the electric field, the stress intensity factor is increased and crack growth resumes; and (4) this model can predict the extent of fatigue crack growth. In contrast to the conventional perception of (mechanical) fatigue, the fatigue crack growth in ferroelectrics under cyclic electric loading is a step by step cleavage process caused by a domain switching sequence that generates a cyclic driving stress field near the crack tip. © 1998 Published by Elsevier Science Ltd. All rights reserved.

Keywords: A. Electric fatigue; A. Crack propagation and arrest; B. Ferro-electric material; B. Cyclic loading; B. Crack mechanics

1. Introduction

Ferroelectric ceramics have been widely employed in many applications, such as electromechanical sensors, transducers and actuators. One critical problem that limits

* Corresponding author. Fax: 0086 1062 562768; e-mail: yw-dem@mail.tsinghua.edu.cn

the device performance is the fatigue degradation associated with the electric cycling. Experiments by Cao and Evans (1994) and Lynch et al. (1995) revealed that cyclic crack growth could be induced under an alternating electric field. Experimental observation (Lynch et al., 1995) indicated that the electric fatigue crack growth arises from a series of cleavage processes in the absence of applied mechanical loading, while in the case of mechanical fatigue test the specimen presents a fractography characterized by inelastic deformation and fretting. The following question is raised: is the electric-field-induced fatigue crack growth caused by electric breakdown, or is it a consequence of the stress field near the crack tip? Though material factors influencing electric-field-induced fatigue behavior of ferroelectrics, including the composition, grain size, and pores (Jiang et al. 1994a,b; Jiang and Cross, 1993) have been studied experimentally, hardly any mechanistic analyses on the electric fatigue crack growth have been reported. It is essential to understand and quantify the electric-field-induced fatigue crack growth in ferroelectrics so that their fatigue life can be predicted.

The first attempt of fracture mechanics analysis for ferroelectrics was based on the linear piezoelectric constitutive equations. Many investigators explored that approach in the past several years (e.g., Pak, 1990; Suo et al., 1992; Zhang et al., 1998). A negative energy release rate is found for an insulating crack under an electric field. This would exclude the electric-field-induced fracture in ferroelectrics, in contradiction with the experimental observation of crack-like growth in multi-layer ferroelectric actuators. Ferroelectrics are known to exhibit strong nonlinear and hysteresis behavior at a large field strength. This effect becomes pronounced around a defect due to the field concentration. To predict failure behavior accurately, the nonlinear effect associated with the ferroelectrics must be incorporated. Several models taking into account the nonlinear effect have been proposed in the recent past. Yang and Suo (1994) and Hao et al. (1996) modeled the electrostrictive ferroelectrics and derived the stress intensity factors for the flaws around the electrode edge under electric loading. Gao et al. (1997) and Fulton and Gao (1997) investigated the effect of electric yielding based on the strip saturation model.

From the microscopic point of view, domain switching (90° and 180°) is the source of non-linearity, and causes a hysteresis loop between the electric displacement and the electric field, and a butterfly loop between the strain and the electric field. Experiments have shown that domain switching also plays an important role in the toughness variation of ferroelectrics (see Pisarenko et al., 1985 and Mehta and Virkar, 1990). A micromechanics model (Yang and Zhu, 1998; Zhu and Yang, 1997) is proposed to evaluate the effect of combined mechanical and electrical loading on crack growth under the small scale domain switching condition, in the sense that the applied loading is not high enough to induce global switching. The concentrated stress and electric fields around the flaw are found to switch the domains therein. The switched domains induce incompatible strain under the constraint of the unswitched material and consequently alter the stress distribution near the flaw.

The present paper will invoke the small scale domain switching model to study the fatigue crack growth driven by cyclic electric loading. A mechanism of fatigue crack growth induced by electric loading should contain the following ingredients: (1) how

an electric field induces fracture (2) by what mechanism the crack arrests and (3) why the crack growth resumes when the electric field is reversed. The plan of the paper is as follows: we start with the description of the small scale domain switching model in section 2. Section 3 will provide an electric-field-induced fracture analysis for a stationary crack. The result indicates that both the positive and the negative electric fields will initiate the crack. However, the effect by a negative electric field is nine times as large as that by a positive one. Section 4 provides a step-by-step analysis to quantify the fatigue crack growth, following the sequences of polarization switches. A steady state analysis will be given to determine the stabilized fatigue crack growth rate. Concluding remarks are given in section 5.

2. Small scale domain switching model

2.1. Domain switching

The ferroelectrics is modeled as an agglomerate of ferroelectric tetragonal domains. For an individual domain, a sufficiently strong electric field may rotate its polarization direction by either 90 or 180°, termed 90 or 180° domain switching. Consider the case of plane strain with domain switching in x_1-x_2 plane. As shown in Fig. 1, the initial polarization direction of a domain forms an angle ϕ with x_1 axis. For 90° domain switching, the polarization switching vector ΔP_i can be expressed as

$$\Delta P_i = \sqrt{2}P_s \begin{Bmatrix} \cos(\phi \pm \frac{3}{4}\pi) \\ \sin(\phi \pm \frac{3}{4}\pi) \end{Bmatrix} \quad (1)$$

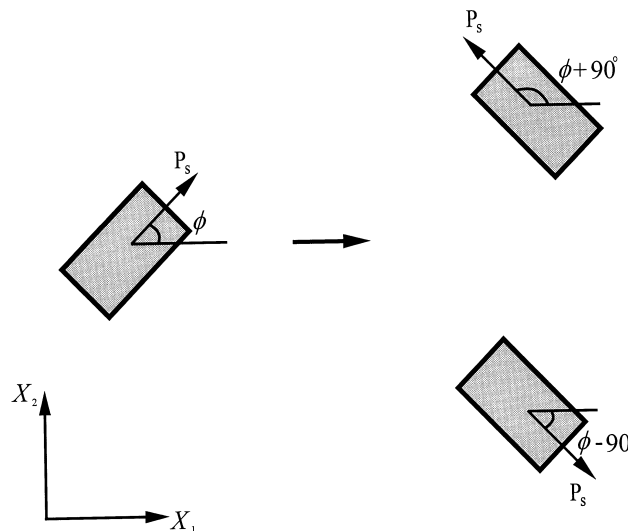


Fig. 1. Two variants of 90° domain switching.

where P_s is the spontaneous polarization. The plus and minus signs in eqn (1) correspond to two possible variants: the domain switches 90° anti-clockwise or clockwise. The switching strain tensor is the same for both cases

$$\Delta\varepsilon_{ij} = \gamma_s \begin{bmatrix} -\cos 2\phi & -\sin 2\phi \\ -\sin 2\phi & \cos 2\phi \end{bmatrix} \quad (2)$$

where γ_s denotes the spontaneous strain associated with 90° switching.

For 180° switching, the switching strain is zero and the polarization switch vector is

$$\Delta P_i = -2P_s \begin{Bmatrix} \cos \phi \\ \sin \phi \end{Bmatrix}. \quad (3)$$

An energy based switching criterion was proposed by Hwang et al. (1995). A 180° switching is irrelevant of stress and activated if the electrical work exceeds a threshold value

$$E_i \Delta P_i \geq 2P_s E_c \quad (4)$$

where E_i denotes the electric field vector, and E_c the coercive field. If the 90° domain switching needs to overcome the same energy barrier $2P_s E_c$, it occurs when the electrical work plus the mechanical work satisfy the following condition

$$\sigma_{ij} \Delta\varepsilon_{ij} + E_i \Delta P_i \geq 2P_s E_c. \quad (5)$$

If two or more directions meet the switching criterion, the domain will switch to the direction in which the work for switching maximizes.

2.2. Toughness variation induced by domain switching

Attention is focused on the situation where the small scale switching condition prevails (Yang and Zhu, 1998; Zhu and Yang, 1997). Cao and Evans (1994) remarked that electric-field-induced fatigue crack growth might arise in regions where field concentrations exist, even though the overall field is below the coercive field. Suppose that the applied loading is low enough so that the bulk of the ceramics is linearly dielectric, except for a small switching zone in the flaw vicinity. The switched domains induce incompatible strain under the constraint of the unswitched material and consequently induce a stress field. The stress intensity factor at the crack tip can be evaluated in the spirit of transformation toughening (see McMeeking and Evans, 1982).

For the poled ferroelectrics, the polarization directions of all domains are roughly aligned with the poling direction. Accordingly, the switching strain is uniform in the entire switching zone. Switching strain induces a thin layer of the accommodating body force T_i on the boundary Γ_s of the switching zone. The deviatoric nature of the switching strain, see eqn (2), leads to

$$T_i = \frac{Y}{1+\nu} \Delta\varepsilon_{ij} n_j \quad (6)$$

where Y denotes Young's modulus, ν Poisson's ratio and the vector n_i the outward normal of Γ_s . The stress intensity factor at the crack tip K_{tip} is evaluated by

$$K_{\text{tip}} = \oint_{\Gamma_s} T_i h_i d\Gamma \quad (7)$$

where h_i is the near tip weight function

$$h_i(r, \theta) = \frac{1}{2(1-\nu)\sqrt{2\pi r}} \begin{cases} \cos \frac{\theta}{2} \left(2\nu - 1 + \sin \frac{\theta}{2} \sin \frac{3\theta}{2} \right) \\ \sin \frac{\theta}{2} \left(2 - 2\nu - \cos \frac{\theta}{2} \cos \frac{3\theta}{2} \right) \end{cases}. \quad (8)$$

3. Electric-field-induced fracture

Consider a crack perpendicular to the poling direction, namely $\phi = 90^\circ$. The electric field applied along the poling direction is defined as the positive electric field, and the one against it the negative electric field. Here we ignore the piezoelectric effect. The square root singular electric field for an insulating crack in a linear dielectric (Suo, 1991) can be invoked

$$\begin{cases} E_1 \\ E_2 \end{cases} = \frac{\pm K_E}{\sqrt{2\pi r}} \begin{cases} -\sin \frac{\theta}{2} \\ \cos \frac{\theta}{2} \end{cases} \quad (9)$$

where K_E is the electric intensity factor and is always positive. The positive and negative signs in (9) correspond to the positive and negative electric fields, respectively.

3.1. Electric-field-induced fracture under a positive electric field

We first discuss the case under a positive electric field. Substituting the positive electric field and the polarization switching vector into the switching criterion, one obtains the shape of the switching zone, denoted by $r(\theta)$ in the polar coordinate system originated from the crack tip. In estimating the shape of the switching zone, we regard the effect of switching-induced-stress as secondary. Thus the switching criterion only involves the electric field. Both 180° and 90° domain switchings are relevant in determining the switching zone geometry. Under a positive electric field, however, the condition of $\sqrt{r} \geq 0$ excludes 180° switching, and leaves only the possibility of 90° switching. Two possible variants of 90° switching exist, namely the domain may switch 90° clockwise or anti-clockwise. The actual switching will select the direction associated with a larger electrical work $\Delta P_i E_i$ for reorientation, or equivalently the switching will occur in the direction with higher algebraic value of

$r(\theta)$. Furthermore, the condition of $\sqrt{r} \geq 0$ determines the range of the angle θ for the switching zone. As shown in Fig. 2, the shape of the switching zone is given by

$$r = r_0 \cos^2\left(\frac{3}{4}\pi - \frac{|\theta|}{2}\right) \quad |\theta| \in \left(\frac{\pi}{2}, \pi\right) \quad (10)$$

where the length parameter

$$r_0 = \left(\frac{K_E}{2\sqrt{\pi E_c}}\right)^2 \quad (11)$$

scales the domain switching zone around the crack tip.

The stress intensity factor at the crack tip is obtained by summing two contributions: one is from the traction over the crack surface Γ_{s1} , and the other from the traction over the curved switching zone boundary Γ_{s2} , then by multiplying the result by a factor 2 due to the symmetry of the upper and the lower switching zones. The contribution from the crack surface traction along Γ_{s1} is easy to calculate and given by

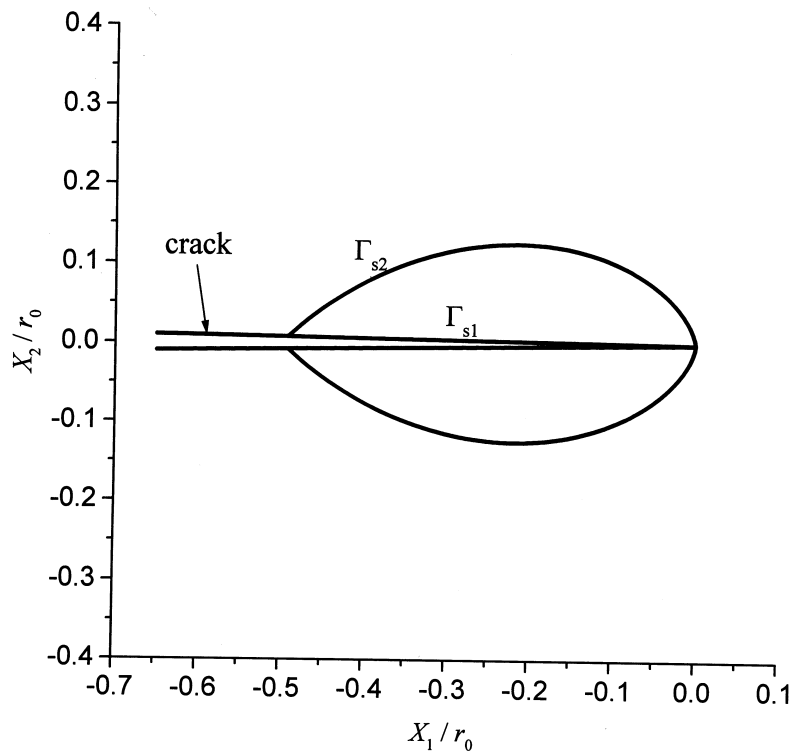


Fig. 2. 90° switching zone driven by a positive electric field.

$$K_{\text{tip}}^{(1)} = \frac{1-\nu}{2\pi} \eta K_E \quad (12)$$

where η is a group of material parameters

$$\eta = \frac{Y\gamma_s}{(1-\nu^2)E_c}. \quad (13)$$

Substituting the geometry of the switching zone boundary eqn (10) into eqn (A2) in the appendix (take the amount of crack growth Δa as zero), one obtains an explicit expression of $K_{\text{tip}}^{(2)}$ by the traction on Γ_{s2}

$$K_{\text{tip}}^{(2)} = \frac{16\nu-15}{32\pi} \eta K_E. \quad (14)$$

The stress intensity factor at the crack tip under a positive electric field is summed as

$$K_{\text{tip}} = 2(K_{\text{tip}}^{(1)} + K_{\text{tip}}^{(2)}) = \frac{\eta}{16\pi} K_E. \quad (15)$$

The crack tip stress intensity factor K_{tip} scales with the applied electric intensity factor K_E . Fracture occurs when K_{tip} reaches the intrinsic fracture toughness K_{IC} of the material at the paraelectric phase. For ferroelectric ceramics, the material constants have the following representative values $Y = 80$ GPa, $\gamma_s = 0.002$, $\nu = 1/3$, $E_c = 0.36$ MV/m and $K_{\text{IC}} = 1$ MPa \sqrt{m} (see Hwang et al., 1995). The threshold of electric intensity factor for electric-field-induced fracture is $K_E = 0.1$ MV/ \sqrt{m} .

3.2. Electric-field-induced fracture under a negative electric field

Domain switching effect under a negative electric field will be evaluated in this subsection. Both 180 and 90° domain switching should be considered. If only 90° domain switching occurs, the switching zone assumes the following shape

$$r = r_0 \cos^2\left(\frac{3}{4}\pi + \frac{|\theta|}{2}\right) \quad (16)$$

which is bounded by the solid line shown in Fig. 3. If only 180° domain switching occurs, the switching zone is bounded by the dash-dot line shown in Fig. 3.

$$r = 2r_0 \cos^2 \frac{\theta}{2}. \quad (17)$$

In determining the actual domain switching direction (90 or 180°), we select the switching direction as the one with higher algebraic value of $r(\theta)$. It follows that 180° switching occurs in the frontal zone ($|\theta| \leq \pi/2$) of the crack, while 90° switching occurs in the rear ($|\theta| > \pi/2$). As shown in Fig. 3, the area shaded with the inclined solid lines represents the 90° switching zone, while the one shaded with the inclined dash lines the 180° switching zone.

Since a 180° switching produces little strain, evaluation of the switching effect will

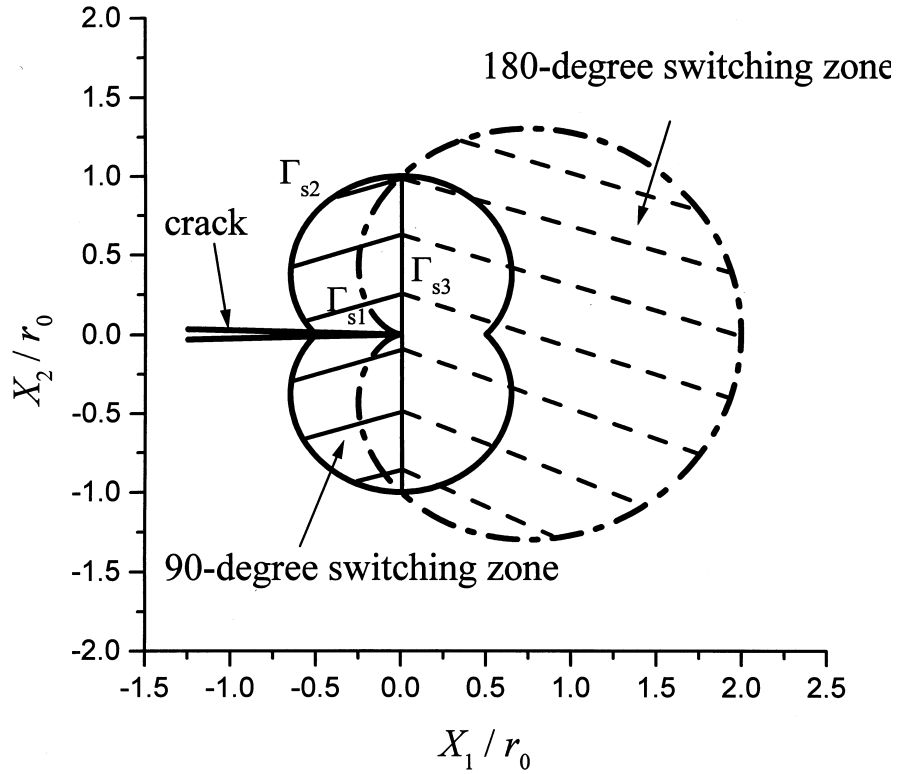


Fig. 3. 90° and 180° switching zones driven by a negative electric field.

be made along the boundary of the 90° switching zone. The contribution from the traction over the crack surface Γ_{s1} is given by

$$K_{\text{tip}}^{(1)} = \frac{1-\nu}{2\pi} \eta K_E. \quad (18)$$

The tractions along the curved section Γ_{s2} and vertical section Γ_{s3} yield the stress intensity factors $K_{\text{tip}}^{(2)}$ and $K_{\text{tip}}^{(3)}$ (see appendix, let Δa be zero)

$$K_{\text{tip}}^{(2)} = \frac{-3}{32\pi} \eta K_E \quad (19)$$

$$K_{\text{tip}}^{(3)} = \frac{4\nu-1}{8\pi} \eta K_E. \quad (20)$$

The net stress intensity factor induced at the crack tip by a negative electric field is

$$K_{\text{tip}} = 2(K_{\text{tip}}^{(1)} + K_{\text{tip}}^{(2)} + K_{\text{tip}}^{(3)}) = \frac{9\eta}{16\pi} K_E. \quad (21)$$

Note that a negative electric field also induces a tensile stress field ahead of the crack tip. Comparing eqn (21) with eqn (15), one finds that switch-induced toughness degradation under a negative electric field is nine times as severe as that under a positive electric field. The physical origin of this difference is understood as follows: the polarization direction of domains near the crack tip forms acute angles with the positive electric field vectors but blunt angles with the negative ones. The state of the polarization direction of a domain aligning with the electric field is energetically favorable, then the domain switching is much easier under a negative electric field. Consequently, the electric-field-induced fracture becomes more pronounced under a negative electric field of the same magnitude of K_E . This result is essential in understanding the cause of electric-field-induced fatigue crack growth under an alternating electric field, as will be examined in the next section.

4. Electric-field-induced fatigue crack growth

Under an alternating electric field, the field concentrated around the crack causes the ferroelectrics to undergo cyclic local domain switching. Driven by the switching induced stress field, the crack experiences a repeated process of initiation, growth, arrest and re-initiation.

4.1. Step-by-step analysis

4.1.1. Crack initiation

Consider a stationary crack under a negative electric field. The 180° switching occurs in the frontal zone of the crack, while the 90° switching occurs in the rear. The shape of 90° switching zone is depicted in Fig. 4(a). The stress intensity factor due to the switching was furnished in eqn (21). Given the electric intensity factor K_E , the crack will initiate if $K_{\text{tip}} > K_{\text{IC}}$. It will extend by cleavage since plasticity is not involved during fracture. For typical ferroelectric material constants listed in section 3, the threshold electric intensity for crack initiation is $0.011 \text{ MV}/\sqrt{m}$.

4.1.2. Crack growth and arrest

As the crack extends, the electric field around the advancing crack tip will induce further domain switching. The toughness variation due to the 90° switching consists of three parts. The contribution from the crack surface traction is given by

$$K_{\text{tip}}^{\text{surface}}(\Delta a) = \frac{Y\gamma_s}{1+\nu} \sqrt{\frac{2\Delta a + r_0}{\pi}}. \quad (22)$$

The other two parts are from the traction along the boundary of newly formed switching zone associated with crack growth, denoted by $K_{\text{tip}}^{\text{frontal}}(\Delta a)$, and that along the boundary of the residual zone translating a distance Δa to the wake, denoted by $K_{\text{tip}}^{\text{wake}}(\Delta a)$. The stress intensity factor at the crack tip, as a function of the crack increment Δa , is given by

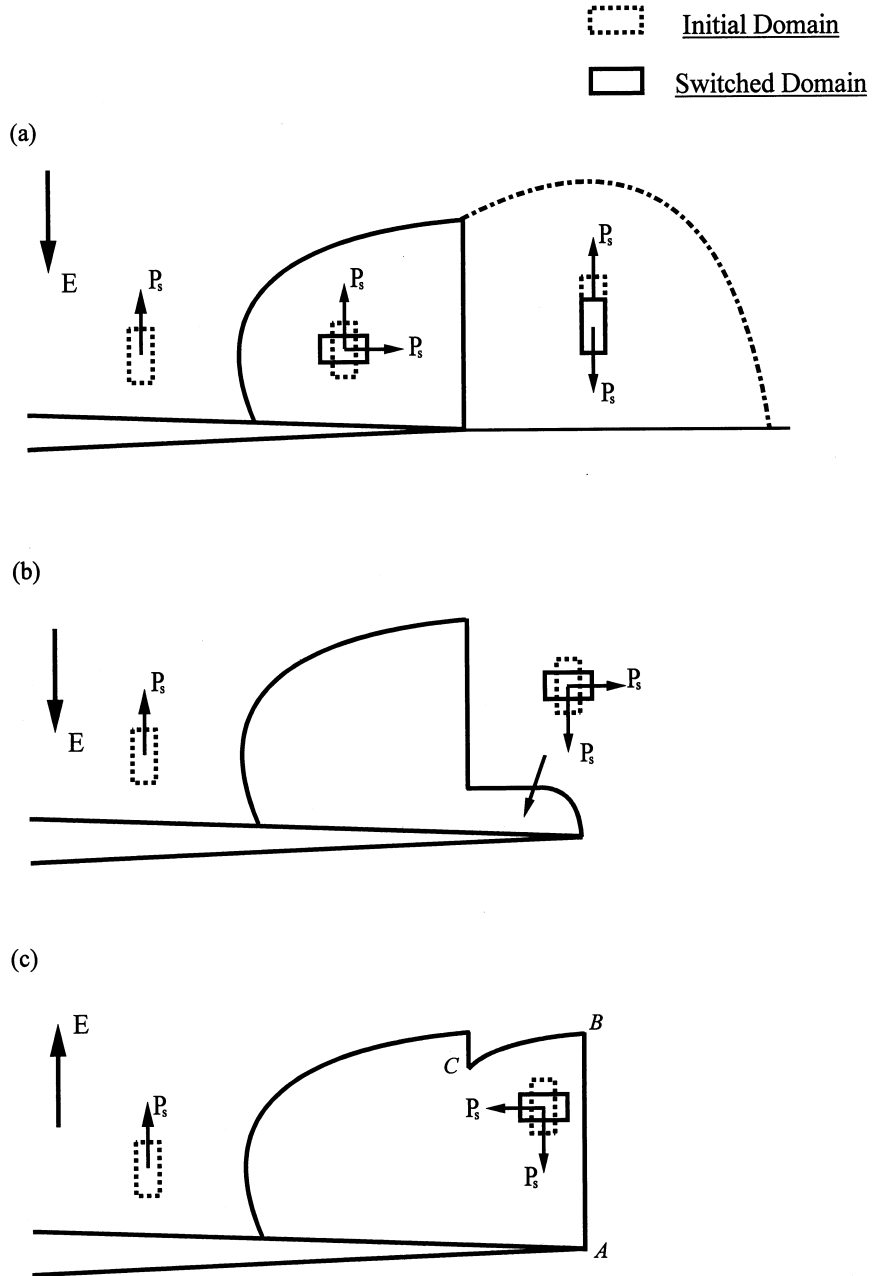


Fig. 4. Schematic illustration of switching zones for electric-field-induced fatigue crack propagation. (a) initiation; (b) growth and arrest; (c) re-initiation.

$$K_{\text{tip}}(\Delta a) = 2[K_{\text{tip}}^{\text{surface}}(\Delta a) + K_{\text{tip}}^{\text{frontal}}(\Delta a) + K_{\text{tip}}^{\text{wake}}(\Delta a)]. \quad (23)$$

The factor 2 in the above equation comes from the symmetry of the switching zone.

As mentioned above, 180° switching occurs in the frontal zone prior to crack initiation. As the crack extends, it will enter the area where 180° switching has occurred. Thus, the calculation of $K_{\text{tip}}^{\text{frontal}}(\Delta a)$ should follow the fracture analysis for ferroelectrics under a *positive* electric field. The boundary of newly formed switching zone is described by eqn (16), with θ ranging from the initial angle $\pi/2$ to the angle θ_c determined by the condition of $|r(\theta_c) \cos \theta_c| = \Delta a$. The stress intensity factor at the crack tip is given by

$$K_{\text{tip}}^{\text{frontal}}(\Delta a) = \frac{\eta K_E}{8\sqrt{2}\pi} \left[(3-4\nu) \cos\left(\theta - \frac{\pi}{4}\right) - \frac{3}{4} \cos\left(2\theta - \frac{\pi}{4}\right) + \frac{1}{8} \cos\left(4\theta - \frac{\pi}{4}\right) \right]_{\pi/2}^{\theta_c}. \quad (24)$$

As the crack continues to extend, the curved boundary will reach its maximum height. The angle marking the maximum height is $\frac{5}{6}\pi$ by the condition of $d/d\theta(r \sin \theta) = 0$. With further crack extension, a horizontal segment connecting the point of the maximum height with the initial switching zone is formed, as shown in Fig. 4(b). The stress intensity factor is the sum of contributions from the curved and the horizontal parts and given by

$$K_{\text{tip}}^{\text{frontal}}(\Delta a) = \frac{\eta K_E}{16\pi} \left\{ \frac{9}{16}(\sqrt{3}-1) - \left[\frac{3-4\nu + \cos \theta}{\sqrt{\sin \theta}} \cos \frac{\theta}{2} \right]_{\tan^{-1}(r_0/8\Delta a)} \right\} \quad (25)$$

In calculating $K_{\text{tip}}^{\text{wake}}(\Delta a)$, we assume that the switched domains in the wake will not undergo a secondary 90° switching. That is, for an observer traveling with the crack tip, the wake translates backward with its shape unchanged. The contribution to the stress intensity factor can be expressed in a general form

$$K_{\text{tip}}^{\text{wake}}(\Delta a) = \Omega(\Delta a) \eta K_E \quad (26)$$

where $\Omega(\Delta a)$ is a function of the crack extension Δa and can be determined by numerical integration (see appendix). Figure 5 shows the K_{tip} versus the crack growth Δa curve. In the sample calculation, we take the electric intensity as $0.04 \text{ MV}/\sqrt{m}$. The induced initial stress intensity factor $K_{\text{tip}}(0)$ is $3.58 \text{ MPa}\sqrt{m}$, see point *a* in Fig. 5. As the crack grows, $K_{\text{tip}}(\Delta a)$ decreases monotonically. The crack arrests at $K_{\text{tip}}(\Delta a_{\text{arrest}}) = K_{\text{IC}}$, see point *b* in Fig. 5.

4.1.3. Crack re-initiation

Upon the reversal of the electric field, the polarization directions of domains near the arrested crack tip form blunt angles with the electric field, and domain switching re-activates. A new boundary of frontal switching zone is formed, as shown in Fig. 4(c). The fracture analysis under a *negative* electric field will be invoked to compute the switching effects of newly formed vertical segment \overline{AB} and curved portion \overline{BC} . The

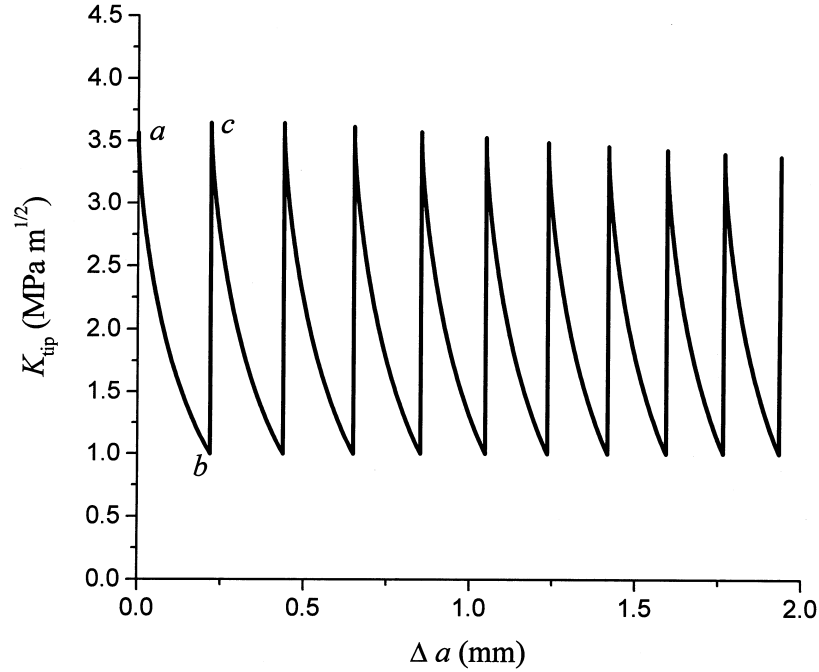


Fig. 5. Variation of stress intensity at the crack tip, $K_{\text{tip}}(\Delta a)$ vs crack growth.

curve \overline{BC} has an angular span from $\pi/2$ to the angle θ_a , the latter is determined by the condition of $|r(\theta_a) \cos \theta_a| = \Delta a_{\text{arrest}}$. The stress intensity factor contributed from the newly formed frontal zone is given by

$$K_{\text{tip}}^{\text{frontal}}(\Delta a) = \frac{\eta K_E}{8\pi} \left\{ 2\nu + \frac{1}{16} + \frac{1}{\sqrt{2}} \left[(4\nu - 3) \cos\left(\theta_a - \frac{3\pi}{4}\right) + \frac{3}{4} \cos\left(2\theta_a - \frac{3\pi}{4}\right) - \frac{1}{8} \cos\left(4\theta_a - \frac{3\pi}{4}\right) \right] \right\}. \quad (27)$$

The calculation of stress intensity factor induced by other portions of the zone boundary is the same as the crack growth analysis. As shown in Fig. 5, $K_{\text{tip}}(\Delta a)$ jumps from point b , corresponding to the arrested state, to point c , indicating that the newly switched domains re-initiate the crack. The process of initiation, growth, arrest and re-initiation repeats itself, leading to cyclic crack growth. The $K_{\text{tip}}(\Delta a)$ curve in the subsequent electric loading cycles will adopt the qualitative variation as that in the first field reversal. The curve of $K_{\text{tip}}(\Delta a)$ associated with crack growth has a zigzag shape, as shown in Fig. 5. Figure 6 plots the crack increment in each electric field reversal versus the number of reversals. As shown in the figure, the crack extends rapidly in the initial stage and then slows down. As the field reversal number increases, the crack will enter a stabilized growth stage and advance at a constant growth rate.

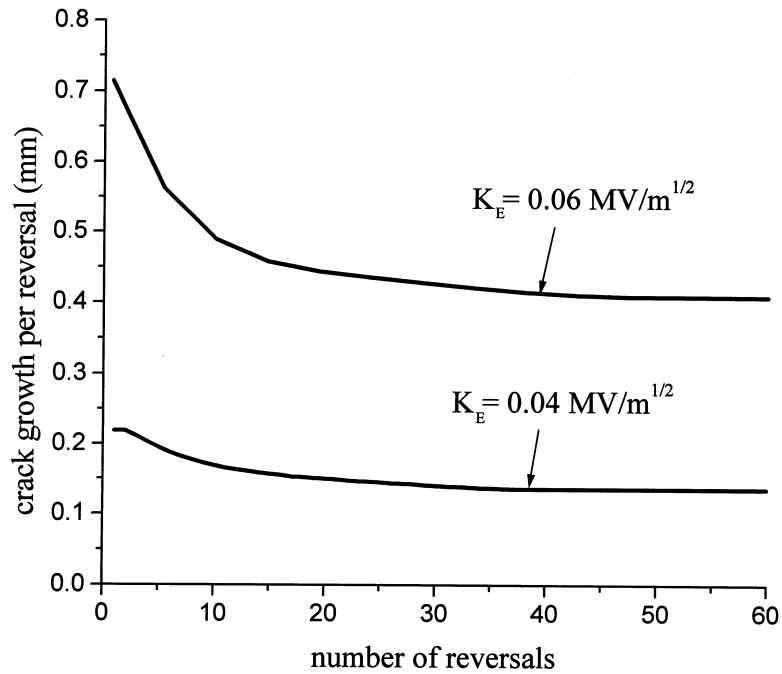


Fig. 6. Crack growth per electric field reversal vs the number of field reversals.

This result is in qualitative agreement with the experimental observation by Lynch et al. (1995).

4.2. Stabilized cyclic crack growth

The crack increment for each electric field reversal under a stabilized growth state will be given in this subsection for different magnitudes of electric loading. The computation is similar to the step-by-step analysis except that a fully developed wake of height $H = r_0$ is adopted. A simplified configuration is shown in Fig. 7. The wake

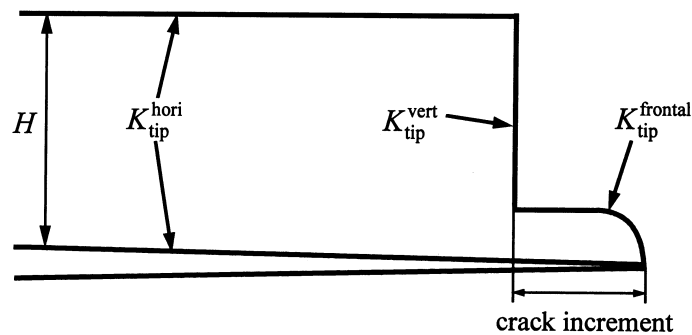


Fig. 7. Simplified configuration for stabilized cyclic crack growth.

is represented by a strip of switched domains appended to the crack surface. The stress intensity factor induced by the frontal zone, denoted by $K_{\text{tip}}^{\text{frontal}}(\Delta a)$, was given by eqn (24) or eqn (25). The contribution from the vertical segment, denoted by $K_{\text{tip}}^{\text{vert}}(\Delta a)$, can be determined numerically as described in the appendix. The contributions from the top boundary of the semi-infinite strip and the crack surface are explicitly summed as

$$K_{\text{tip}}^{\text{hor}}(\Delta a) = \frac{\eta K_E}{4\sqrt{2\pi}} \frac{\sin \frac{\theta_H}{2}}{\sqrt{\sin \theta_H}} (3 - 4\nu - \cos \theta_H). \quad (28)$$

The angle θ_H in eqn (28) corresponds to the starting point of the top horizontal boundary of the strip. For a given electric intensity K_E , the cracking increment for each electric field reversal can be implicitly determined by

$$K_{\text{tip}}(\Delta a) = 2[K_{\text{tip}}^{\text{frontal}}(\Delta a) + K_{\text{tip}}^{\text{vert}}(\Delta a) + K_{\text{tip}}^{\text{hor}}(\Delta a)] = K_{\text{IC}}. \quad (29)$$

The result from numerical calculation is shown in Fig. 8 for two representative values

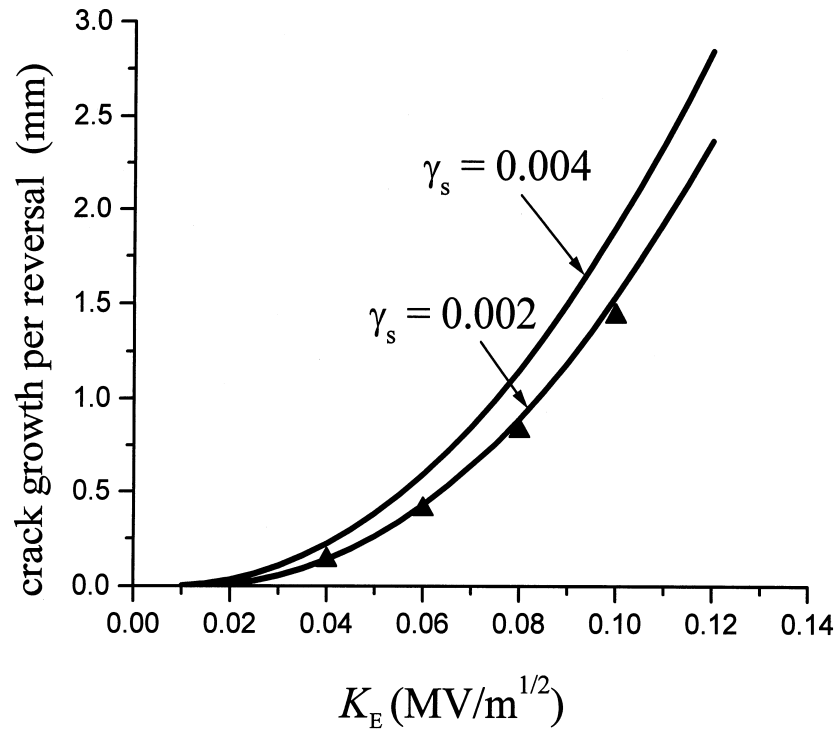


Fig. 8. Curve of stabilized cyclic crack growth rate. Triangles represent the result from step-by-step analysis ($\gamma_s = 0.002$).

0.002 and 0.004 of γ_s . A threshold electric field exists for electric-field-induced fatigue crack growth. With the rise of either the electric field or the spontaneous switching strain, the crack increment per field reversal increases for the stabilized growth state. The triangles in the figure represent the result from the step-by-step analysis, where γ_s is taken as 0.002. The stabilized estimate for crack increment forms a tight upper-bound, as it should, to the prediction from the step-by-step analysis under the same spontaneous switching strain.

5. Concluding remarks

A quantitative mechanistic model for electric-field-induced fatigue crack growth is advanced in this work. The analysis lends theoretical support to the experimental observations that the fatigue crack growth proceeds as a step-by-step cleavage process driven by the cyclic electric loading induced stress field. Electric-field-induced fracture and fatigue are analyzed within the framework of small scale domain switching. For ferroelectrics poled along a direction perpendicular to the crack, we are able to show quantitatively that both the positive and negative electric fields will initiate the crack. The stress intensity factor at the crack tip induced by a negative electric field is nine times as large as that by a positive one. Based on this result, various steps of fatigue crack propagation, such as crack initiation, growth, arrest and re-initiation, are explained by the sequence of polarization switching.

During the repeated domain switching, microcracks may develop and degrade the ferroelectrics, as discussed by Jiang et al. (1994) and Zhang and Jiang (1995). The attention of the present paper is rather focused on the driving force for the fatigue crack propagation, while the effect of microcracking can be treated as the degradation of K_{IC} . The present treatment might ignore the effect of crack interaction. The interaction between the switching induced microcracks and the main crack in ferroelectrics is a worthwhile research issue in the future.

Appendix

The stress intensity factor at the crack tip induced by the accommodating body force on the switching zone boundary for a growing crack will be given here. For the poled ferroelectrics discussed in the paper, the angles of the polarization directions of all domains are $\pi/2$. The accommodating body force will be

$$T_1 = \frac{Y\gamma_s}{1+\nu}n_1, T_2 = \frac{-Y\gamma_s}{1+\nu}n_2. \quad (\text{A1})$$

Substituting eqn (A1) and eqn (8) into eqn (7) of the text, one obtains the expression of K_{tip}

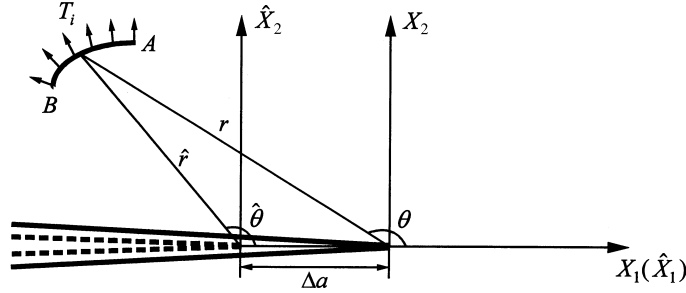


Fig. 9. Coordinate systems used to calculate the stress intensity factor for a crack with an increment Δa .

$$K_{\text{tip}} = \frac{Y\gamma_s}{2\sqrt{2\pi(1-\nu^2)}} \oint_{\Gamma_s} \left[\cos \frac{\theta}{2} \left(2\nu - 1 + \sin \frac{\theta}{2} \sin \frac{3\theta}{2} \right) n_1 - \sin \frac{\theta}{2} \left(2 - 2\nu - \cos \frac{\theta}{2} \cos \frac{3\theta}{2} \right) n_2 \right] \frac{d\Gamma}{\sqrt{r}}. \quad (\text{A2})$$

The function $r(\theta)$ measures the boundary of the switching zone in the coordinates attached to the moving crack tip.

The computation of K_{tip} will be carried out in the coordinates \hat{r} and $\hat{\theta}$ whose origin locates at the initial crack tip, as shown in Fig. 9. Consider a segment \overline{AB} of zone boundary described by coordinates \hat{r} and $\hat{\theta}$, where $\hat{\theta}$ varies from $\hat{\theta}_A$ to $\hat{\theta}_B$. Two sets of coordinates differ by a translation of Δa , and are related by (see Fig. 9)

$$r = \sqrt{\hat{r}^2 + (\Delta a)^2 - 2\hat{r}\Delta a \cos \hat{\theta}}, \quad \theta = \pi - \arcsin \left(\frac{\hat{r} \sin \hat{\theta}}{r} \right). \quad (\text{A3})$$

A line element on the segment \overline{AB} is given by

$$d\Gamma = \sqrt{\hat{r}^2 + \left[\frac{d\hat{r}(\hat{\theta})}{d\hat{\theta}} \right]^2} d\hat{\theta} \quad (\text{A4})$$

and the outward normal is such that

$$n_1 = \left[\hat{r} \cos \hat{\theta} + \sin \hat{\theta} \frac{d\hat{r}(\hat{\theta})}{d\hat{\theta}} \right] / \sqrt{\hat{r}^2 + \left[\frac{d\hat{r}(\hat{\theta})}{d\hat{\theta}} \right]^2}$$

$$n_2 = \left[\hat{r} \sin \hat{\theta} - \cos \hat{\theta} \frac{d\hat{r}(\hat{\theta})}{d\hat{\theta}} \right] / \sqrt{\hat{r}^2 + \left[\frac{d\hat{r}(\hat{\theta})}{d\hat{\theta}} \right]^2}. \quad (\text{A5})$$

Substituting eqns (A3), (A4) and (A5) into (A2) and numerically integrating (A2) from $\hat{\theta}_A$ to $\hat{\theta}_B$, the stress intensity factor contributed from the segment \overline{AB} for a growing crack with an increment of Δa will be obtained. In several special cases, explicit expressions of stress intensity factor can be derived as shown in the text.

Acknowledgement

The authors are grateful for the support by National Natural Foundation of China.

References

- Cao, H.C., Evans, A.G., 1994. Electric-field-induced fatigue crack growth in piezoelectric ceramics. *J. Am. Ceram. Soc.* 77, 1783–1786.
- Fulton, C.C., Gao, H., 1997. Electrical nonlinearity in fracture of piezoelectric ceramics. *Appl. Mech. Rev.* 50, S56–S63.
- Gao, H., Zhang, T.Y., Tong, P., 1997. Local and global energy rates for an electrically yielded crack in piezoelectric ceramics. *J. Mech. Phys. Solids* 45, 491–510.
- Hao, T.H., Gong, X., Suo, Z., 1996. Fracture mechanics for the design of ceramic multilayer actuators. *J. Mech. Phys. Solids* 44, 23–48.
- Hwang, S.C., Lynch, C.S., McMeeking, R.M., 1995. Ferroelectric/ferroelastic interactions and a polarization switching model. *Acta Metall. Mater.* 43, 2073–2084.
- Jiang, Q., Subbarao, E.C., Cross, L.E., 1994a. Effect of composition and temperature on electric fatigue of La-doped lead zirconate titanate ceramics. *J. Appl. Phys.* 75, 7433–7443.
- Jiang, Q., Subbarao, E.C., Cross, L.E., 1994b. Grain size dependence of electric fatigue behavior of hot pressed PLZT ferroelectric ceramics. *Acta Metall. Mater.* 42, 3687–3694.
- Jiang, Q., Cross, L.E., 1993. Effect of porosity on electrical fatigue behavior in PLZT and PZT ceramics. *J. Mater. Sci.* 28, 4536–4543.
- Lynch, C.S., Yang, W., Collier, L., Suo, Z., McMeeking, R.M., 1995. Electric field induced cracking in ferroelectric ceramics. *Ferroelectrics* 166, 11–30.
- McMeeking, R.M., Evans, A.G., 1982. Mechanics of transformation toughening in brittle materials. *J. Am. Ceram. Soc.* 65, 242–246.
- Mehta, K., Virkar, A.V., 1990. Fracture mechanism in ferroelectric-ferroelastic lead zirconate titanate (Zr:Ti = 0.54:0.46) ceramics. *J. Am. Ceram. Soc.* 73, 567–574.
- Pak, Y.E., 1990. Crack extension force in a piezoelectric material. *J. Appl. Mech.* 57, 647–653.
- Pisarenko, G.G., Chushko, V.M., Kovalev, S.P., 1985. Anisotropy of fracture toughness of piezoelectric ceramics. *J. Am. Ceram. Soc.* 68, 259–265.
- Suo, Z., Kuo, C.-M., Barnett, D.M., Willis, J.R., 1992. Fracture mechanics for piezoelectric ceramics. *J. Mech. Phys. Solids* 40, 739–765.
- Suo, Z., 1991. Mechanics concepts for failure in ferroelectric ceramics. In: Srinivasan, A.V. (Ed.), *Smart Structures and Material*. ASME, New York, pp. 1–6.
- Yang, W., Suo, Z., 1994. Cracking in ceramic actuators caused by electrostriction. *J. Mech. Phys. Solids* 42, 649–663.
- Yang, W., Zhu, T., 1998. Switch-toughening of ferroelectrics under electric field. *J. Mech. Phys. Solids* 46, 291–311.
- Zhang, T.Y., Qian, C.F., Tong, P., 1998. Linear electro-elastic analysis of a cavity of a crack in a piezoelectric material. *Int. J. Solids Struct.* 35, 2121–2149.
- Zhang, Y., Jiang, Q., 1995. Twinning-induced stress and electric field concentrations in ferroelectric ceramics. *J. Am. Ceram. Soc.* 78, 3290–3296.
- Zhu, T., Yang, W., 1997. Toughness variation of ferroelectrics by polarization switch under non-uniform electric field. *Acta Mater.* 45, 4695–4702.